


Sign-reversal superconducting gaps revealed by phase-referenced quasiparticle interference of impurity-induced bound states in $(\text{Li}_{1-x}\text{Fe}_x)\text{OHFe}_{1-y}\text{Zn}_y\text{Se}$

Qiangqiang Gu, Qingkun Tang, Siyuan Wan, Zengyi Du, Xiong Yang, Huan Yang,* Qiang-Hua Wang, Hai Lin, Xiyu Zhu, and Hai-Hu Wen†

*National Laboratory of Solid State Microstructures and Department of Physics,
Collaborative Innovation Center of Advanced Microstructures, Nanjing University, Nanjing 210093, China*

 (Received 28 March 2018; revised manuscript received 16 September 2018; published 11 October 2018)

By measuring the spatial distribution of differential conductance near nonmagnetic impurities on Fe sites, we have obtained the quasiparticle interference (QPI) patterns in the $(\text{Li}_{1-x}\text{Fe}_x)\text{OHFe}_{1-y}\text{Zn}_y\text{Se}$ superconductor with only electron Fermi surfaces. By taking the Fourier transform on these patterns, we investigate the scattering features between the two circles of electron pockets formed by folding or hybridization. We treat the data by using the recent theoretical approach [Chi *et al.*, [arXiv:1710.09089](https://arxiv.org/abs/1710.09089)], which is specially designed for the impurity-induced bound states. It is found that the opposite superconducting gap signs on the two electron pockets can be directly visualized by the phase-referenced QPI technique, indicating that the Cooper pairing is induced by the repulsive interaction. Our results show that this method is also applicable for data measured for multiple impurities, which provides an easy and feasible way for detecting the gap function of unconventional superconductors.

DOI: [10.1103/PhysRevB.98.134503](https://doi.org/10.1103/PhysRevB.98.134503)

I. INTRODUCTION

The discovery of iron-based superconductors [1] provides us a second example of unconventional high-temperature superconductors. It is categorized as unconventional because a lot of unique features have been found. For example, the parent phase of $R\text{FeAsO}$ (R = rare earth elements) and $A\text{EFe}_2\text{As}_2$ ($A\text{E}$ represents the alkaline earth metals Ba, Sr, Ca, etc.) have the long range antiferromagnetic (AFM) orders [2,3]. The superconductivity emerges when this long-range AFM order is suppressed. Plenty of evidence indicates that superconductivity has been mediated by AFM spin fluctuations in the pairing process [4]. Theoretically, it was proposed that the pairing may be established by the pair-scattering of two electrons with opposite momenta between the hole and electron pockets [5,6] leading to the so-called sign reversal s -wave gap, namely the s^\pm -pairing manner. This picture, originally proposed for the FeAs-based system with both electron and hole pockets, has been actually supported by several important experiments, such as the quasiparticle interference (QPI) in $\text{FeTe}_{1-x}\text{Se}_x$ [7] and inelastic neutron scattering [8]. We have also done the experiments of scanning tunneling microscopy/spectroscopy (STM/STS) measurements on nonmagnetic Cu impurities in $\text{Na}(\text{Fe}_{0.96}\text{Co}_{0.03}\text{Cu}_{0.01})\text{As}$ and found clear evidence of the in-gap bound states providing strong support of the s^\pm -pairing [9]. In addition, a bosonic mode was observed outside the superconducting coherence peaks in at least two systems [10] with the mode energy Ω scaling with the superconducting transition temperature T_c in

the way $\Omega \approx 4.3k_B T_c$. This has been naturally explained as a consequence of the s^\pm -pairing gap.

It seems that the model of s^\pm -pairing is so far so good for the systems with both electron and hole pockets. However, new challenges come out for some later discovered FeSe-based systems, such as the FeSe monolayer thin film [11], $(\text{Li}_{1-x}\text{Fe}_x)\text{OHFeSe}$ [12,13], etc., which seems to show the absence of hole pockets in the center of the Brillouin zone [14,15]. The key question is whether we still have sign reversal gaps among the electron pockets. If it exists, what is the configuration of the gap pattern, two candidates would be the nodeless d -wave pairing [16,17] and the bonding-antibonding s^\pm pairing [18]. Recently, we have adopted a phase-referenced (PR) proposal [19] by Hirschfeld, Altenfeld, Eremin, and Mazin (HAEM) for measuring the gap sign, and found the evidence of sign-reversal gaps [20] in the system $(\text{Li}_{1-x}\text{Fe}_x)\text{OHFe}_{1-y}\text{Zn}_y\text{Se}$. This method is relying on the determination of a sophisticated quantity associated with the real part of antisymmetrized interband Fourier transformed (FT)-QPI. It is expected that this quantity will be coherently enhanced in the region between two gaps. Furthermore, a careful calibration is needed to obtain the phase message by implementing the phase-correction method [21].

Very recently, another method was proposed to judge the gap sign problem in LiFeAs with both electron and hole pockets. Namely, the phase information can be validly extracted from the impurity-induced bound states [22,23]. It seems that this new method is sensitive and straightforward. In the present work, we operate QPI measurements around one single impurity in Zn-doped $(\text{Li}_{1-x}\text{Fe}_x)\text{OHFeSe}$ and also in a large area with multiple impurities in $(\text{Li}_{1-x}\text{Fe}_x)\text{OHFeSe}$. Applying this new method for one single impurity, we find out the robust proof of gap sign reversal directly visualized on the two electron pockets. Furthermore, in a system with

*huanyang@nju.edu.cn

†hhwen@nju.edu.cn

multiple and identical impurities, we can recover the similar results as the case of one single impurity when carrying out the phase-correction of these impurities. Our results indicate that the unconventional Cooper pairing in $(\text{Li}_{1-x}\text{Fe}_x)\text{OHFeSe}$ is originated from the on-site Coulomb interaction, as previously proposed in the FeAs-based superconductors.

II. EXPERIMENTAL METHOD

The single crystals of $(\text{Li}_{1-x}\text{Fe}_x)\text{OHFeSe}$ and $(\text{Li}_{1-x}\text{Fe}_x)\text{OHFe}_{1-y}\text{Zn}_y\text{Se}$ are synthesized by hydrothermal ion-exchange method [12,20,24]. The value of y in $(\text{Li}_{1-x}\text{Fe}_x)\text{OHFe}_{1-y}\text{Zn}_y\text{Se}$ analyzed by x-ray energy dispersive spectrum is about 2%. The dc magnetization at 20 Oe shows that the critical temperatures of $(\text{Li}_{1-x}\text{Fe}_x)\text{OHFeSe}$ and Zn-doped samples are 36.4 K and 33.4 K, respectively.

STM/STS measurements are carried out by a scanning tunneling microscope (USM-1300, Unisoku Co., Ltd.) with the ultrahigh vacuum, low-temperature, and high-magnetic field. All the samples were cleaved at room temperature in an ultrahigh vacuum of 1×10^{-10} Torr, and then transferred into the low-temperature microscope head immediately. The electrochemically etched tungsten tips were used during all measurements. To raise the signal-to-noise ratio in dI/dV spectra, a typical lock-in technique was used with an ac modulation of 0.4 mV at 987.5 Hz. All data in the paper were taken at 1.5 K.

III. RESULTS

A. Theoretical model of bound-state based PR-QPI

The Bogoliubov quasiparticles with the momentum and energy (\mathbf{k}, E) can be elastically scattered by defects to another state (\mathbf{k}', E) , forming a standing wave with the wave vector $\mathbf{q} = \mathbf{k}' - \mathbf{k}$. Such standing waves can be easily observed by STM in the real space from QPI measurement. The measured differential conductance mapping $g(\mathbf{r}, E)$ is proportional to the local density of states (LDOS) when the spatial variation of the tunneling matrix element is irrelevant. Then the detailed information in q space can be obtained by applying the Fourier transformation to QPI data, which reflects the scatterings in k space. The obtained FT-QPI $g(\mathbf{q}, E)$ is a complex parameter, and can be expressed as $g(\mathbf{q}, E) = |g(\mathbf{q}, E)|e^{i\theta_{\mathbf{q},E}}$, with $\theta_{\mathbf{q},E}$ the phase of the standing wave.

Recently, a PR-QPI method based on the analysis of the bound states was proposed to determine the gap symmetry [22,23], and the model is based on the PR-QPI near one single impurity. The model yields the PR-QPI differential conductivity at positive and negative energies, which read as

$$g_r(\mathbf{q}, +E) = |g(\mathbf{q}, +E)|, \quad (1)$$

$$g_r(\mathbf{q}, -E) = |g(\mathbf{q}, -E)| \cos(\theta_{\mathbf{q},-E} - \theta_{\mathbf{q},+E}). \quad (2)$$

As one can see, $\theta_{\mathbf{q},+E}$ in the above equations is used as a referenced phase when compared to $\theta_{\mathbf{q},-E}$. Then the phase difference term can be expressed as

$$\begin{aligned} & \cos(\theta_{\mathbf{q},-E} - \theta_{\mathbf{q},+E}) \\ &= \cos\theta_{\mathbf{q},-E} \cos\theta_{\mathbf{q},+E} + \sin\theta_{\mathbf{q},-E} \sin\theta_{\mathbf{q},+E} \end{aligned}$$

$$\begin{aligned} &= \frac{\text{Re}[g(\mathbf{q}, -E)] \text{Re}[g(\mathbf{q}, +E)]}{|g(\mathbf{q}, -E)| |g(\mathbf{q}, +E)|} \\ &+ \frac{\text{Im}[g(\mathbf{q}, -E)] \text{Im}[g(\mathbf{q}, +E)]}{|g(\mathbf{q}, -E)| |g(\mathbf{q}, +E)|}, \quad (3) \end{aligned}$$

where Re represents the real part of the complex function $g(\mathbf{q}, E)$, and Im represents the imaginary part. The real and imaginary part of FT-QPI $g(\mathbf{q}, E)$ at a certain q is directly given by the Fourier transform. The $g_r(\mathbf{q}, +E)$ is always positive as defined by Eq. (1). Specially, for the nonmagnetic impurity within s^\pm pairing symmetry, the signal of $g_r(\mathbf{q}, -E)$ from sign reversed scattering will change into a negative value at the bound-state energy $-E_B$.

Furthermore, this method can be also used in a system with multiple impurities [22], and here the measured differential conductance mapping $g(\mathbf{r}, E)$ can be converted into

$$g(\mathbf{r}, E) = \sum_j g_s(\mathbf{r} - \mathbf{R}_j, E), \quad (4)$$

where \mathbf{R}_j is the location of the j th impurity, and then $g_s(\mathbf{r} - \mathbf{R}_j, E)$ is the differential conductance mapping by moving the center of the j th impurity to the origin. After a brief mathematical operation [22], we can recover $g_s(\mathbf{q}, E)$ from $g(\mathbf{q}, E)$; namely,

$$g_s(\mathbf{q}, E) = \frac{g(\mathbf{q}, E)}{\sum_j e^{-i\mathbf{q}\cdot\mathbf{R}_j}}. \quad (5)$$

From the equation above, with no complicated calculation concerned, the denominator $\sum_j e^{-i\mathbf{q}\cdot\mathbf{R}_j}$ is only determined by the location of each impurity. As a result, it could be a practical way to obtain $g_s(\mathbf{q}, E)$ directly from $g(\mathbf{q}, E)$, then $g_r(\mathbf{q}, \pm E)$ can be calculated from Eqs. (1) and (2) by replacing the information of $g(\mathbf{q}, E)$ by that of $g_s(\mathbf{q}, E)$. Above all, we can conclude that this phase-sensitive method is applicable both for the case of one single impurity and also for a system with multiple impurities, if a careful calibration is done.

This original bound-state based PR-QPI technique was successfully used to detect the gap sign on LiFeAs from the scattering between the hole and electron pockets [22,23]. However, in $(\text{Li}_{1-x}\text{Fe}_x)\text{OHFeSe}$ [14,15,25] or $(\text{Li}_{1-x}\text{Fe}_x)\text{OHFe}_{1-y}\text{Zn}_y\text{Se}$ [20], the hole pocket is absent near Γ point of the Brillouin zone. Figure 1(a) shows the schematic Fermi surfaces of the LiOH intercalated FeSe compounds, and the size of the electron pockets are taken from our previous experiments [25]. To compare with experiment, we simulate the FT-QPI pattern by applying self-correlation to the Fermi surfaces shown in Fig. 1(a) and assuming a constant intensity everywhere around the Fermi surfaces. In Fig. 1(b), we show the central pattern of the FT-QPI simulation. The two white circles mark the integrated region for experimental bound-state based PR-QPI. The two electron pockets can give rise to two sets of the intrapocket scattering and one set of the inter-pocket scattering, which make the situation complex. It is curious to know whether the PR-QPI method applied for LiFeAs can also be applicable for $(\text{Li}_{1-x}\text{Fe}_x)\text{OHFeSe}$ or $(\text{Li}_{1-x}\text{Fe}_x)\text{OHFe}_{1-y}\text{Zn}_y\text{Se}$ in which the hole pocket is absent.

Hence we constructed a two-orbital tight-binding model to calculate the results in this system. The two-electron Fermi

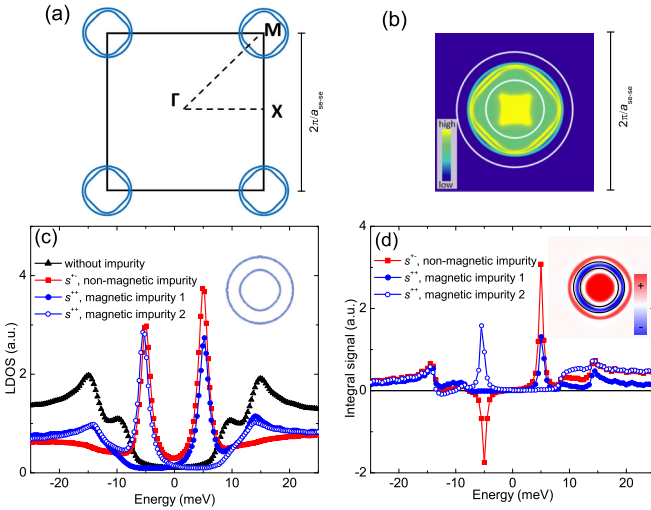


FIG. 1. (a) The schematic Fermi surfaces in 2-Fe Brillouin zone. The two electron pockets with moderate hybridization are located around each M point, and the sizes of the electron pockets are determined from the measured FT-QPI results [25]. (b) The simulation of FT-QPI intensity by using self-correlation to (a). For clarity, only the central pattern with small q is presented here. The selected region between the two white solid circles is chosen as $0.37\pi/a_{\text{Se-Fe}} < q < 0.74\pi/a_{\text{Se-Fe}}$, which is used as the integrated region for experimental bound-state-based PR-QPI. (c) The simulated tunneling spectra at a position without any impurities or at different kinds of impurities. The scattering potential $V_s = -0.3$ eV for the nonmagnetic impurity; $V_s = -0.12$ eV and $V_m = 0.21$ eV for magnetic impurity 1; $V_s = -0.088$ eV and $V_m = -0.22$ eV for magnetic impurity 2. The inset shows the Fermi surfaces constructed by a tight-binding two-orbital model in the calculation. (d) Energy-dependent PR-QPI signals within ± 25 meV for three kinds of impurities within the pairings of s^{++} and s^{\pm} . The inset shows the calculated bound-state based PR-QPI signal $g_r(\mathbf{q}, -E)$ image at $-E_B$ for the nonmagnetic impurity in s^{\pm} pairing, and the integrated region is chosen between the two black circles in the inset with the range of $0.375\pi/a_{\text{Se-Fe}} < q < 0.5\pi/a_{\text{Se-Fe}}$, which concerns mainly the signal from inter-pocket scattering.

surfaces in the calculations are simplified to two concentric circles with slight deformation, which are shown in the inset of Fig. 1(c). The outer electron pocket has the similar size as the experimental result [25], while the inner pocket is smaller than the experimental result in order to explicitly distinguish the contributions of three scattering channels. Two isotropic superconducting gaps, i.e., 8.5 meV and 14 meV, are assigned to the inner and outer Fermi pockets [25], respectively. Then we utilize a standard T-matrix approach [26] to simulate LDOS near a single impurity. The unperturbed Green's function in the real space can be formulated as

$$G_0(\mathbf{r}, \mathbf{r}', E) = \frac{1}{N} \sum_{\mathbf{k}} G_0(\mathbf{k}, E) e^{i\mathbf{k} \cdot (\mathbf{r} - \mathbf{r}')}, \quad (6)$$

where N is the number of the unit cells. $G_0(E) \equiv G_0(\mathbf{r}, \mathbf{r}, E) = 1/N \sum_{\mathbf{k}} G_0(\mathbf{k}, E)$, and then the T-matrix for the multiple scattering by a single impurity is defined as

$$T^{-1}(E) = (V_s \sigma_3 + V_m \sigma_0)^{-1} - G_0(E), \quad (7)$$

where σ_i is the i^{th} Pauli matrix, V_s is the scalar potential, V_m is the magnetic potential ($V_m = 0$ for nonmagnetic impurity). Then the spatial evolution of LDOS in real space with an impurity located at the center can be obtained by

$$\begin{aligned} \rho(\mathbf{r}, E) &= \rho_0(\mathbf{r}, E) + \delta\rho(\mathbf{r}, E) \\ &= -\frac{1}{2\pi} \text{ImTr}(\tau_0 + \tau_3)[G_0(E) \\ &\quad + G_0(\mathbf{r}, \vec{0}, E)T(E)G_0(\vec{0}, \mathbf{r}, E)], \end{aligned} \quad (8)$$

where τ_i is the Pauli matrix spanning Nambu space, and $\vec{0}$ represents the position of the impurity which is in the center of the image.

The calculated tunneling spectra are shown in Fig. 1(c). The superconducting tunneling spectrum is similar to the experimental ones [20,25], and the bound-state peaks are very obvious on the spectra at the nonmagnetic impurity site in the case of s^{\pm} pairing or at the magnetic impurity sites in the case of s^{++} pairing. The inset of Fig. 1(d) shows the image of the bound-state-based PR-QPI signal $g_r(\mathbf{q}, -E)$ from the calculated $\rho(\mathbf{r}, E)$ at the bound-state energy $-E_B$ for nonmagnetic impurity in s^{\pm} pairing. One can find that the signal is obviously negative for the inter-pocket scattering in the area between the two black circles in the inset of Fig. 1(d); however, the signal for the intrapocket scattering is positive from both the inner or outer pockets. These features are consistent with the expectations. Using the integrated area between the two circles in the inset of Fig. 1(d), we have calculated the integral of PR-QPI signal within ± 25 meV, and the results for the three kinds of impurities are plotted in Fig. 1(d). For s^{\pm} -pairing symmetry with a nonmagnetic impurity, the integral signal becomes negative near $-E_B$ with negative peak exactly locating at the negative bound state energy. In contrast, we find no sign-reversed features in the integral signal for the magnetic impurity within s^{++} pairing symmetry no matter where the bound-state peak position is.

We also check our calculation results by HAEM PR-QPI method, and the $\delta\rho^-(E)$ signal from the inter-pocket scattering always dominates the integral signal at energies between the two superconducting gaps even if the integrated region contains three different scattering channels. However, for the bound-state-based PR-QPI technique used here, the integral result is very sensitive to the integrated region. At the negative bound-state energy, the area of the positive values from intrapocket scattering of the outer pocket is larger than that of the negative values from inter-pocket scattering. Therefore, the total integral signal will be positive in bound-state-based PR-QPI method from our calculation when the integral area covers all the three scattering channels. The reason for this may be due to the very simplified two-orbital model of the calculation, so we did the integral mainly over the inter-pocket scattering to get a quantitative result for the bound-state-based PR-QPI method as mentioned above. The conclusion is that the antiphase signal from the inter-pocket scattering will emerge near $-E_B$ only if there is a gap sign reverse, although the calculation is carried out on the two concentric electron pockets with similar sizes. If the integral signal around the scattering channels are negative near $-E_B$ for nonmagnetic impurity in the experiment, there should be a sign change gap between two electron pockets. In addition, we can conclude from the calculation that the PR-QPI method based on the

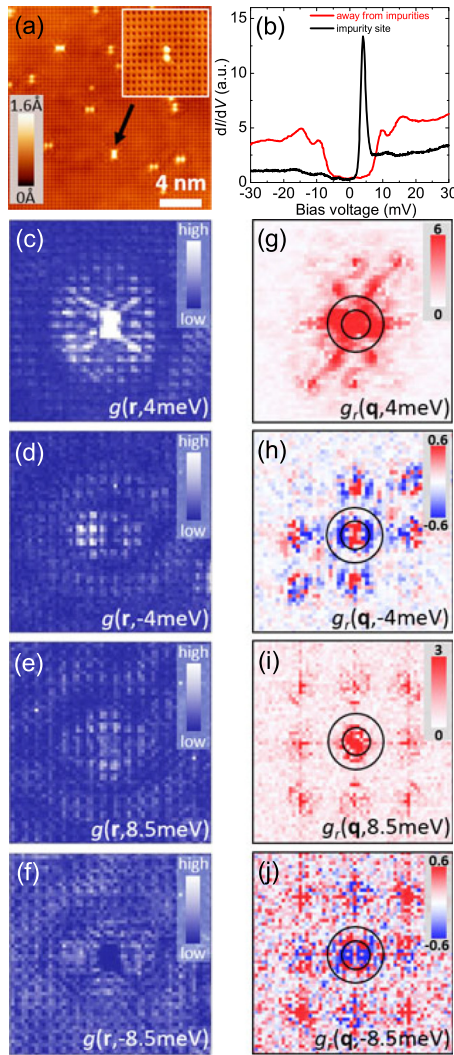


FIG. 2. (a) A typical topographic image of Se terminated layer in $(\text{Li}_{1-x}\text{Fe}_x)\text{OHFe}_{1-y}\text{Zn}_y\text{Se}$ measured with bias voltage $V_b = 30$ mV and tunneling current $I_t = 50$ pA. The arrow indicates a well-isolated Fe-site impurity, and the inset shows the rescanned image with higher resolution around this impurity ($V_b = 30$ mV, $I_t = 100$ pA). (b) Tunneling spectra measured at the center of the impurity marked by the arrow in (a) and far away from impurities ($V_b = 30$ mV, $I_t = 100$ pA). Differential conductance mappings $g(\mathbf{r}, E)$ (c)–(f) and bound-state-based phase-referenced QPI patterns $g_r(\mathbf{q}, E)$ (g)–(j) at different energies. These data obtained from the QPI images measured with 64×64 pixels in the area with the topography shown in the inset of Fig. 2(a). The integral processes in (g)–(j) are carried out in the regions between two solid circles, which are the same as those shown in Fig. 1(b).

bound states [22,23] is applicable at and near the bound state peak energy, not effective like the HAEM method, which is sensitive to the energies between two gaps [19] since there are some differences between the two methods.

B. The bound-state based PR-QPI method applied on one single impurity situation

Figure 2(a) shows a typical atomically resolved topography of a $(\text{Li}_{1-x}\text{Fe}_x)\text{OHFe}_{1-y}\text{Zn}_y\text{Se}$ sample after cleavage, and

the Se terminated surface shows a square lattice with lattice constant close to 3.7 Å. The impurities on Fe sites make the surface topography near them behave as the dumbbell shapes [20]. The inset of Fig. 2(a) shows the topographic image with a well-isolated impurity in the center. The spectrum measured at an impurity-free position is shown in Fig. 2(b), and the spectrum is featured by a standard “U” shape indicating an s -wave pairing without any node crossing the Fermi surfaces. One can also easily distinguish two gaps $\Delta_1 = 14$ meV and $\Delta_2 = 8.5$ meV from the spectrum; therefore, the material behaves as a multigap superconductor like $\text{Ba}_{0.6}\text{K}_{0.4}\text{Fe}_2\text{As}_2$ [27], LiFeAs [28], etc. Moreover, the impurity induced bound state peaks appear at $\pm E_B = \pm 4$ meV, while the peak has almost negligible amplitude at the negative energy. This impurity is proved to be a nonmagnetic one distinguished by the non-shift of the peak energy under the magnetic field of 11 T [20].

The QPI patterns were measured at different energies within ± 24 meV in the region whose topography is shown in the inset of Fig. 2(a), and the nonmagnetic impurity is located in the center of the image. After carrying out some mathematical procedures based on Eqs. (1) and (2), we can get a series of PR-QPI patterns from the raw data. In Figs. 2(c)–2(j), we present the differential conductance mappings $g(\mathbf{r}, E)$ and resultant patterns of $g_r(\mathbf{q}, E)$ at typical energies $E = \pm 4$ meV and ± 8.5 meV, which are at the impurity bound state energies and the smaller gap $\pm \Delta_2$, respectively. Obvious twofold symmetry can be observed in the resultant bound-state-based PR-FT-QPI images. The reason is that the Fe-site impurity sits just under the midpoint between the two nearest-neighbored Se atoms on the surface, which naturally lowers down the fourfold symmetry of the square lattice and this can get support from the topographic image near the impurity. The two circles in each figure have the same sizes as those in Fig. 1(b), and the region between them contains the main scattering intensity of the intra- or interpocket scattering. It is not strange that $g_r(\mathbf{q}, E)$ at some positive energy is positive everywhere, because it is the absolute value according to Eq. (1). However, negative values seem to be dominant in the concerned region between two circles at $E = -4$ meV, which indicates that the selected area contains the sign reversal interpocket scattering. The area with negative value of $g_r(\mathbf{q}, E < 0)$ shrinks when $|E|$ increases, and then the positive and negative areas are almost balanced near -8.5 meV.

Inferred from the theoretical models and previous experimental results [22,23], the absolute value of PR-QPI signal is enhanced significantly when the energy is close to the in-gap bound state. The major difference is the sign of the PR-QPI signals near the bound-state peak at the negative energies for different kinds of impurities in superconductors with different gap symmetries, i.e., negative for nonmagnetic impurity in a superconductor with sign-reversal gaps and positive for magnetic impurity in a superconductor with sign preserved gaps [23]. To quantitatively describe the feature of PR-QPI pattern in the sample, we calculate the integrals of $g_r(\mathbf{q}, E)$ over the selected area at different energies ranging from -24 meV to $+24$ meV, and plot the experimental result in Fig. 3. One can see that the peaks for integral signal near “ $-E_B$ ” is negative. It should be noted that the integral area for the experiment contains three scattering channels, and here

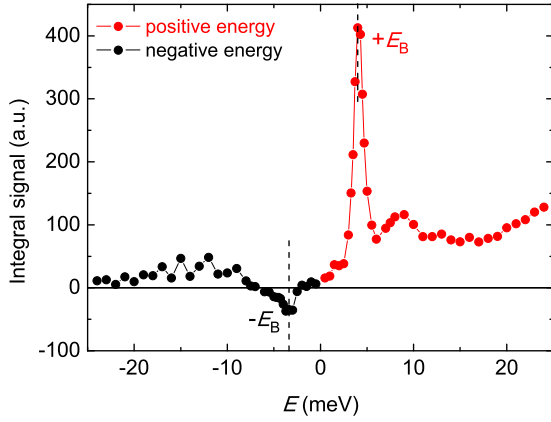


FIG. 3. The integral signal of experimental $g_r(\mathbf{q}, E)$ versus energy. The integrated area in q space is restricted between the two circles shown in Fig. 1(b) or Figs. 2(g)–2(j).

the negative signal finally dominates. It is consistent with the result from nonmagnetic impurity in s^\pm model from our calculation. Accordingly, we believe this is another proof of sign-reversal superconducting gaps between the two electron pockets in $(\text{Li}_{1-x}\text{Fe}_x)\text{OHFe}_{1-y}\text{Zn}_y\text{Se}$ besides our previous one [20].

C. Control experiment on another kind of single impurity

To reinforce the reliability of the analyzing method and also conclusions above, we have carried out a control experiment on another kind of impurity. Figure 4(a) shows a single impurity which is well located at the center in a field of view (FOV) with dimensions of $6\text{ nm} \times 6\text{ nm}$. The impurity pattern is dumbbell shaped as well. In Fig. 4(b), we show the spectra measured at the impurity site under magnetic fields of 0 T and 11 T, respectively. At zero field, one can see that two pairs of bound states peaks emerge at $\pm E_{B1} = \pm 2.7\text{ meV}$ and $\pm E_{B2} = \pm 5.6\text{ meV}$, which is different from the impurity in the previous subsection with only one pair of impurity bound states. The high magnetic field does not shift the peak positions of the in-gap states, manifesting the nonmagnetic character of this impurity [20].

Subsequently, a set of differential conductance mappings were measured in the region shown in Fig. 4(a). The PR-QPI patterns can be calculated from the measured data as Figs. 4(c)–4(f), and the related results are presented in Figs. 4(g)–4(j). One can clearly see that most of the values between the two circles are negative at the energies of -3 meV and -5 meV , which are close to the in-gap bound state energies. Then we calculated the integral signals over the area between the two circles, and the energy evolution of the signal is plotted in Fig. 5. From the resultant curve, these two pairs of the integral signal peaks are located near in-gap state energies marked by $\pm E_{B1}$ and $\pm E_{B2}$, with a sign changing at the positive and negative energy sides. Clearly, the experimental results of the two different impurities are consistent with the theoretical calculation in which there exists a sign-reversal gap between the two electron pockets in $(\text{Li}_{1-x}\text{Fe}_x)\text{OHFe}_{1-y}\text{Zn}_y\text{Se}$.

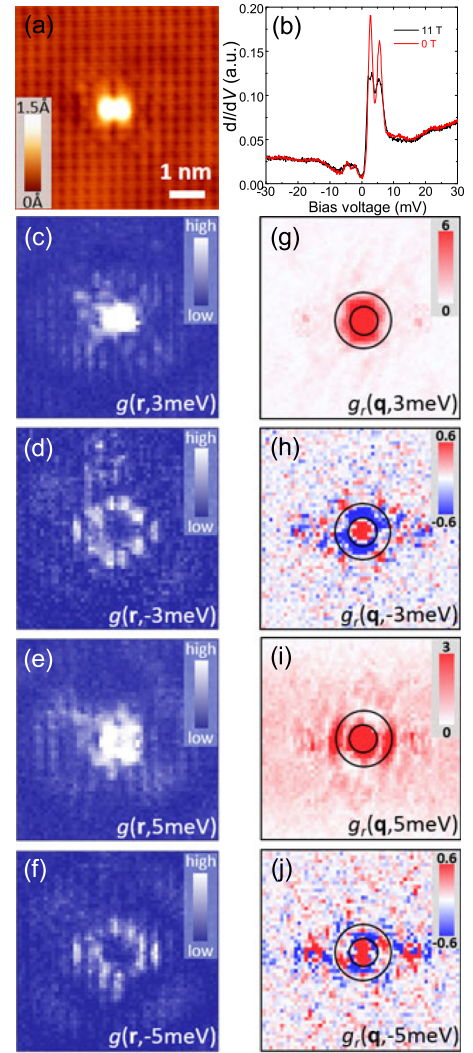


FIG. 4. (a) Topography of another kind of a single impurity located at the center of the image with dimensions of $6\text{ nm} \times 6\text{ nm}$ ($V_b = 30\text{ mV}$, $I_t = 100\text{ pA}$). (b) Tunneling spectra measured on the impurity site under the magnetic fields of 0 T and 11 T, respectively ($V_b = 30\text{ mV}$, $I_t = 100\text{ pA}$). Differential conductance mappings $g(\mathbf{r}, E)$ (c)–(f) and phase-referenced QPI patterns (g)–(j) at $E = \pm 3\text{ meV}$ and $\pm 5\text{ meV}$. The two circles adhered to (g)–(j) are the same sizes as depicted in Fig. 1(b).

D. Same method applied on multiple impurities

Next, we present the data of a new round of experiments on a Zn-free sample with multiple impurities. As shown in Fig. 6(a), plenty of impurities are witnessed in a FOV of $28\text{ nm} \times 28\text{ nm}$ and all defects show similar dumbbell shapes. Tunneling spectra measured at the centers of the two different impurities and at an impurity-free position are presented in Fig. 6(b). The tunneling spectrum measured at the impurity-free position is featured by a “U” shape, which indicates a nodeless gap feature. The clear and sharp coherence peaks reveal the double gaps in the Zn-free samples, and the feature is also very close to the one measured on the Zn-doped samples. Impurities in FOV can be mainly categorized into two kinds, and the symbols for these two kinds are impurity 1 (marked by yellow circle) and impurity 2 (marked by white circle),

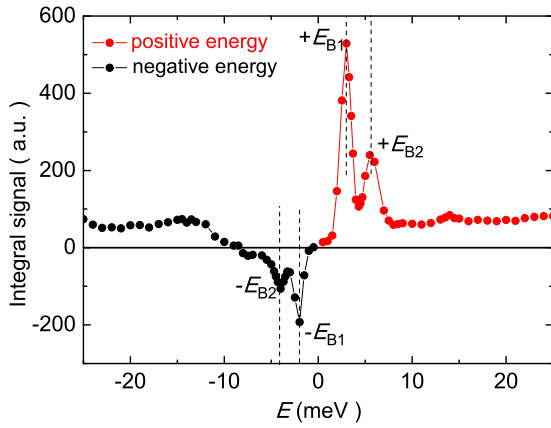


FIG. 5. The integral of $g_r(\mathbf{q}, E)$ versus E varying from -25 meV to $+25$ meV for the impurity shown in Fig. 4(a). The two pairs of peaks located at $\pm E_{B1}$, $\pm E_{B2}$ are attributed to the impurity-induced bound states.

respectively. As for impurity 1, the impurity-induced bound state peaks at the positive energies are much stronger than those at the negative energies, and the situation is reversed with respect to impurity 2. In Figs. 6(c) and 6(d), we display differential conductance mappings measured at energies close to the in-gap state with the smaller peak energy. One can clearly see that there exists an obvious difference between the QPI patterns induced by impurity 1 and impurity 2. Besides, we present another three pairs of mappings at different energies in Figs. 6(e)–6(j). Arising from the synthesis procedure of hydrothermal ion-exchange method with many kinds of elements in $(\text{Li}_{1-x}\text{Fe}_x)\text{OHFeSe}$, these two different kinds of impurities may come from the vacancies of Fe or the substitution of Fe-sites by atoms of other elements, probably the Li atoms.

Therefore, if we want to recover $g_s(\mathbf{q}, E)$ from the QPI measurements for the large area with multiple impurities, it is necessary to mask out one kind of impurities with another kind left. Specifically, the values in the circle surrounding one kind of impurity (1 or 2) with a radius 1.6 nm are substituted by the average value of the whole differential conductance mapping, as a result that there could be only the other kind of identical impurities in the masked mapping. Then we can get a series of PR-QPI patterns referring to Eq. (5) and then Eqs. (1) and (2). To figure out the energy evolution of $g_r(\mathbf{q}, E)$, we present a series of patterns at the negative energies varying from -2.5 meV to -16 meV for impurity 1 in Fig. 7. The patterns at positive energies are not presented here because they are nothing but the absolute values of FT-QPI without extra phase-related information. As we know, the FT-QPI results have some diffuse weights arising from the long-range disorders in real space, so that the pattern with very small q which is concentrated within the inner circle could be complex to analyze. As mentioned above, the selected region between two circles will cover the main scattering intensity of the intra- or inter-pocket scattering. One can clearly see that most of the values in the selected area are negative when the energies are close to impurity-induced in-gap state energies of impurity 1 [Figs. 7(b)–7(d)]. In Fig. 7(f), it is obvious that there are two neighbored contours with positive and negative

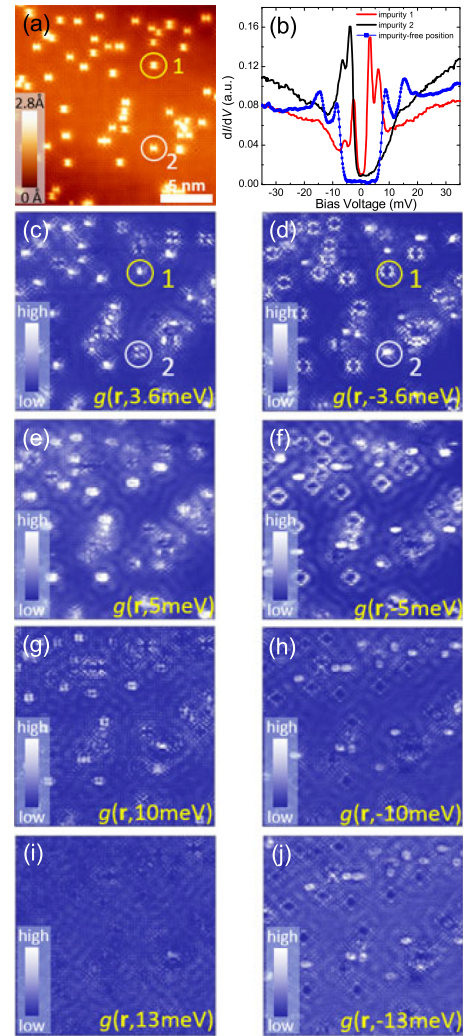


FIG. 6. (a) Topography of a $28 \text{ nm} \times 28 \text{ nm}$ area with plenty of dumbbell shaped impurities in $(\text{Li}_{1-x}\text{Fe}_x)\text{OHFeSe}$ sample ($V_b = 40$ mV, $I_t = 100$ pA). (b) Spectra measured at the centers of two different impurities [marked as 1 and 2 in (a)] and at an impurity-free position ($V_b = 40$ mV, $I_t = 200$ pA). (c)–(j) Differential conductance mappings measured at different energies in the same area as the topography shown in (a). As one can see, impurities in (a) can be mainly categorized into two kinds.

values, respectively, in the selected region, which may be from the different kinds of scatterings if the gap changes its sign for the two electron pockets. When the energy exceeds the larger gap, the positive signals begin to dominate, which may be the signal from the normal state. We then plot the energy-dependent integral signals of $g_r(\mathbf{q}, E)$ for these two kinds of impurities in Fig. 8. As one can see, the signal reaches its extrema at the energies close to the bound state peaks, meanwhile, it does have a sign change for positive and negative energies. This is consistent with the theoretical prediction for the nonmagnetic impurities in an s^\pm pairing superconductor [23]. Thus we have successfully recovered the $g_s(\mathbf{q}, E)$ in a system with multiple impurities, giving strong support for the sign-reversal gaps between the two electron pockets in $(\text{Li}_{1-x}\text{Fe}_x)\text{OHFeSe}$.

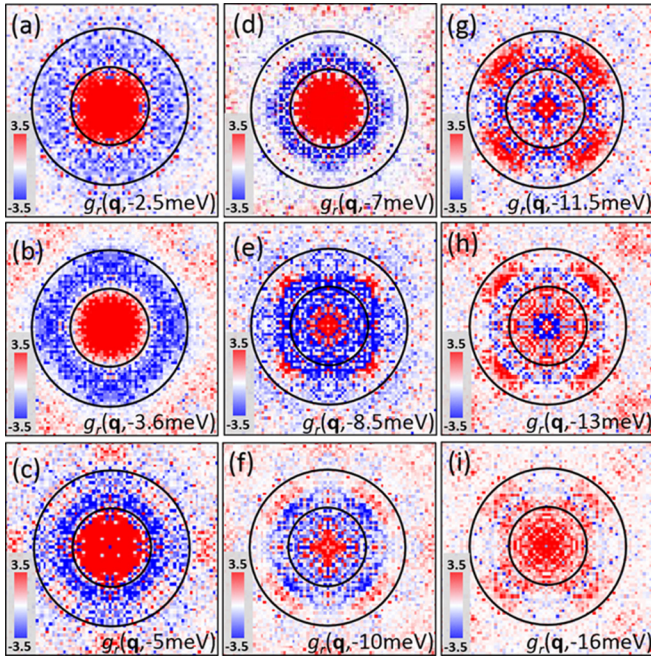


FIG. 7. The phase-referenced QPI patterns of $g_s(\mathbf{q}, E)$ at negative energies for impurity 1. The side length and the selected region between the two circles for integral are the same as those shown in Fig. 1(b).

IV. DISCUSSION

In treating the experimental data, the integral regions are determined carefully according to the simulation based on the topography of the Fermi surface. It should be noted that the signal near $q = 0$ has some diffuse spectral weight which is difficult to interpret, therefore we integrate the FT-QPI intensity within the area between the two circles as shown in Fig. 1(b). We have actually simulated the QPI signal from all possible scattering channels in our previous work [20], and find out that the area between the two circles cover actually the major contributions of the three relevant large- q scattering channels. According to our understanding, although

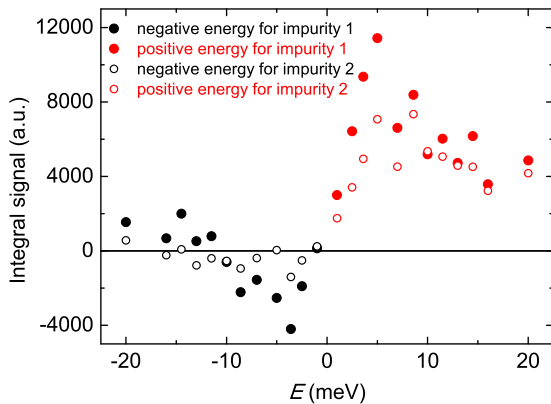


FIG. 8. The integral signal of phase-referenced QPI for impurity 1 and impurity 2. The extrema emerge close to the impurity bound-state energies.

the interband scattering may concern the sign change of order parameters, the intraband scattering should, however, not involve the sign change problem. Because the three circles of FT-QPI as shown in Fig. 1(b) are very close to each other, it is very difficult to distinguish all these scattering channels separately. In this case, what we can do is just to integrate the total signal due to inter- and intraband large- q scatterings, which are well covered by the region between the two concentric circles. In addition, for the case of a single impurity, we should select the isolated one from others as far as possible. In this case, as shown in Figs. 2 and 4, where the scanning area is quite small because of the limited distance from the neighboring impurities, thus the resolution of FT-QPI signal in q space is very limited. The output of FT-QPI will be seriously influenced by the impurity shape or orientation, this would lead to the fluctuation of FT-QPI signal in the q space. The situation is much improved for a large scanning area, as shown in Figs. 6 and 7.

Compared with the case of one single impurity, QPI measurements for a large area with multiple impurities can give us a high resolution in q space and we can obtain more details of the QPI scatterings from the Fermi surfaces. Between the two circles in Fig. 1(b), there are three scattering channels, and two of which are sign-reserved and one is sign-changed. Roughly speaking, these three scattering channels will mix together and then it may hinder for identifying the sign-changed scattering. In fact, specially for the bound state peak energy at -3.6 meV in Fig. 7(b), the selected region is almost covered by the negative values, thus indicating the existence of sign-reversal gaps. As we understand, the scattering of the Bogoliubov quasiparticles with energy E_k and wave-vector k in a superconductor can be characterized by the coherence factors [29], namely

$$u_k = \frac{\Delta_k}{|\Delta_k|} \sqrt{\frac{1}{2} \left(1 + \frac{\varepsilon_k}{E_k} \right)}, \quad v_k = \sqrt{1 - |u_k|^2}, \quad (9)$$

where $|u_k|^2$ and $|v_k|^2$ are the probabilities that Cooper pairs unoccupy and occupy the $\pm k$ state, and ε_k is the kinetic energy. Within the Fermi's golden rule, the scattering probability from k to k' is roughly proportional to $C(k, k') = |u_k u_{k'} - v_k v_{k'}|^2$ for the scalar potential [29,30]. Provided that the scatters are nonmagnetic, the value of $C(k, k')$ for the sign-changed scattering will be much larger than the one for the sign-reserved scatterings at the low excited energy within superconducting gap. Therefore, we can get the strong sign-changed signal mainly from the interpocket scattering with sign-reversal gaps in the PR-QPI pattern near the impurity bound state peaks.

From the experimental data of PR-QPI, we can find that the integral of $g_r(\mathbf{q}, E)$ has a sign changing of the signal peak between the positive and negative energies near the impurity bound states. We can also note that the signals at the high energies become positive both in the single- or multi-impurity situation as shown in Figs. 3, 5, and 8. It should be noted that the sign reversal of PR-QPI signal is based on the phase change originated from the scattering of Bogoliubov quasiparticles within the superconducting gap.

However, the situation for the normal state should be different, i.e., the angles of $\theta_{\mathbf{q},-E}$ and $\theta_{\mathbf{q},E}$ should be similar for normal state quasiparticles. In another words, at high energies beyond superconducting gap, $C(k, k')$ will tend to be a constant 1 both for sign-reversed and reserved processes. Hence, it is not strange that integral signals of $g_s(\mathbf{q}, \pm E)$ become a positive value in the normal state when $|E|$ is much larger than gap values.

In Ref. [20], we have obtained an elusive quantity, the real part of antisymmetrized FT-QPI, which is defined as $\delta g^-(E) = \sum_{\mathbf{q}} \text{Re}[g(\mathbf{q}, +E) - g(\mathbf{q}, -E)]$, and is coherently enhanced within the energy region between two gaps [19]. It provides us a robust evidence of the sign reversal gaps on the two electron pockets in $(\text{Li}_{1-x}\text{Fe}_x)\text{OHFe}_{1-y}\text{Zn}_y\text{Se}$ [20]. This phase-sensitive method is designed for the case of one isolated impurity; as a result, the phase message can not be easily affected by other neighbored impurities in the scanning image. Back to the recently proposed approach [22,23] used in this paper, namely the bound-state based PR- QPI for one single impurity, it is also very helpful to judge the sign problem of the order parameters near the energy of the impurity state. Furthermore, this new approach is applicable for the system with multiple impurities as well and we have successfully recovered the similar result as the measurements of one single impurity.

V. SUMMARY

We performed a series of QPI measurements around a single impurity in $(\text{Li}_{1-x}\text{Fe}_x)\text{OHFe}_{1-y}\text{Zn}_y\text{Se}$. Adopting the newly proposed method of bound-state based PR- QPI, we demonstrate that there exists a sign-reversal gap between the two electron pockets. Furthermore, for the situation in $(\text{Li}_{1-x}\text{Fe}_x)\text{OHFeSe}$ with multiple impurities, the similar results are also obtained which coincide well with the theoretical predictions. Considering a practical case, sometimes it may not be easy to find out one well-isolated impurity, so that the PR-QPI measurements applied for multiple impurities seem to be more realistic and thus provide a practical way to detect the gap function of unconventional superconductors. Our results suggest that the FeSe-based superconductors without hole pockets have a sign reversal of gaps between the two electron pockets, being consistent with the picture of unconventional Cooper pairing mediated by exchanging AFM spin fluctuations.

ACKNOWLEDGMENTS

This work was supported by National Key R & D Program of China (Grant No. 2016YFA0300401), National Natural Science Foundation of China (Grant No. 11534005), and Natural Science Foundation of Jiangsu (Grant No. BK20140015).

-
- [1] Y. Kamihara, T. Watanabe, M. Hirano, and H. Hosono, *J. Am. Chem. Soc.* **130**, 3296 (2008).
- [2] Clarina de la Cruz, Q. Huang, J. W. Lynn, J. Li, W. Ratcliff II, J. L. Zarestky, H. A. Mook, G. F. Chen, J. L. Luo, N. L. Wang, and P. Dai, *Nature (London)* **453**, 899 (2008).
- [3] M. Rotter, M. Tegel, and D. Johrendt, *Phys. Rev. Lett.* **101**, 107006 (2008).
- [4] H. Takeda, T. Imai, M. Tachibana, J. Gaudet, B. D. Gaulin, B. I. Saparov, and A. S. Sefat, *Phys. Rev. Lett.* **113**, 117001 (2014).
- [5] I. I. Mazin, D. J. Singh, M. D. Johannes, and M. H. Du, *Phys. Rev. Lett.* **101**, 057003 (2008).
- [6] K. Kuroki, S. Onari, R. Arita, H. Usui, Y. Tanaka, H. Kontani, and H. Aoki, *Phys. Rev. Lett.* **101**, 087004 (2008).
- [7] T. Hanaguri, S. Niitaka, K. Kuroki, and H. Takagi, *Science* **328**, 474 (2010).
- [8] A. D. Christianson, E. A. Goremychkin, R. Osborn, S. Rosenkranz, M. D. Lumsden, C. D. Malliakas, I. S. Todorov, H. Claus, D. Y. Chung, M. G. Kanatzidis, R. I. Bewley, and T. Guidi, *Nature (London)* **456**, 930 (2008).
- [9] H. Yang, Z. Y. Wang, D. L. Fang, Q. Deng, Q. H. Wang, Y. Y. Xiang, Y. Yang, and H. H. Wen, *Nat. Commun.* **4**, 2749 (2013).
- [10] Z. Y. Wang, H. Yang, D. L. Fang, B. Shen, Q. H. Wang, L. Shan, C. L. Zhang, P. C. Dai, and H. H. Wen, *Nat. Phys.* **9**, 42 (2012).
- [11] Q. Y. Wang, Z. Li, W. H. Zhang, Z. C. Zhang, J. S. Zhang, W. Li, H. Ding, Y. B. Ou, P. Deng, K. Chang, J. Wen, C. L. Song, K. He, J. F. Ji, S. H. Ji, Y. Y. Wang, L. L. Wang, X. Chen, X. C. Ma, and Q. K. Xue, *Chin. Phys. Lett.* **29**, 037402 (2012).
- [12] X. F. Lu, N. Z. Wang, H. Wu, Y. P. Wu, D. Zhao, X. Z. Zeng, X. G. Luo, T. Wu, W. Bao, G. H. Zhang, F. Q. Huang, Q. Z. Huang, and X. H. Chen, *Nat. Mater.* **14**, 325 (2015).
- [13] U. Pachmayr, F. Nitsche, H. Luetkens, S. Kamusella, F. Bruckner, R. Sarkar, H. H. Klauss, and D. Johrendt, *Angew. Chem., Int. Ed. Engl.* **54**, 293 (2015).
- [14] L. Zhao, A. J. Liang, D. N. Yuan, Y. Hu, D. F. Liu, J. W. Huang, S. L. He, B. Shen, Y. Xu, X. Liu, L. Yu, G. D. Liu, H. X. Zhou, Y. L. Huang, X. L. Dong, F. Zhou, K. Liu, Z. Y. Lu, Z. X. Zhao, C. T. Chen, Z. Y. Xu, and X. J. Zhou, *Nat. Commun.* **7**, 10608 (2016).
- [15] X. H. Niu, R. Peng, H. C. Xu, Y. J. Yan, J. Jiang, D. F. Xu, T. L. Yu, Q. Song, Z. C. Huang, Y. X. Wang, B. P. Xie, X. F. Lu, N. Z. Wang, X. H. Chen, Z. Sun, and D. L. Feng, *Phys. Rev. B* **92**, 060504(R) (2015).
- [16] F. Yang, Fa Wang, and D. H. Lee, *Phys. Rev. B* **88**, 100504(R) (2013).
- [17] M. Khodas and A. V. Chubukov, *Phys. Rev. Lett.* **108**, 247003 (2012).
- [18] I. I. Mazin, *Phys. Rev. B* **84**, 024529 (2011).
- [19] P. J. Hirschfeld, D. Altenfeld, I. Eremin, and I. I. Mazin, *Phys. Rev. B* **92**, 184513 (2015).
- [20] Z. Y. Du, X. Yang, D. Altenfeld, Q. Q. Gu, H. Yang, I. Eremin, P. J. Hirschfeld, I. I. Mazin, H. Lin, X. Y. Zhu, and H. H. Wen, *Nat. Phys.* **14**, 134 (2018).
- [21] P. O. Sprau, A. Kostin, A. Kreisler, A. E. Bohmer, V. Taufour, P. C. Canfield, S. Mukherjee, P. J. Hirschfeld, B. M. Andersen, and J. C. Séamus Davis, *Science* **357**, 75 (2017).
- [22] S. Chi, W. N. Hardy, R. X. Liang, P. Dosanjh, P. Wahl, S. A. Burke, and D. A. Bonn, *arXiv:1710.09088*.
- [23] S. Chi, W. N. Hardy, R. X. Liang, P. Dosanjh, P. Wahl, S. A. Burke, and D. A. Bonn, *arXiv:1710.09089*.
- [24] X. L. Dong, K. Jin, D. N. Yuan, H. X. Zhou, J. Yuan, Y. L. Huang, W. Hua, J. L. Sun, P. Zheng, W. Hu, Y. Y. Mao,

- M. W. Ma, G. M. Zhang, F. Zhou, and Z. X. Zhao, *Phys. Rev. B* **92**, 064515 (2015).
- [25] Z. Y. Du, X. Yang, H. Lin, D. L. Fang, G. Du, J. Xing, H. Yang, X. Y. Zhu, and H. H. Wen, *Nat. Commun.* **7**, 10565 (2016).
- [26] Q. H. Wang and D. H. Lee, *Phys. Rev. B* **67**, 020511(R) (2003).
- [27] L. Shan, Y. L. Wang, B. Shen, B. Zeng, Y. Huang, A. Li, D. Wang, H. Yang, C. Ren, Q. H. Wang, S. H. Pan, and H. H. Wen, *Nat. Phys.* **7**, 325 (2011).
- [28] T. Hanaguri, K. Kitagawa, K. Matsubayashi, Y. Mazaki, Y. Uwatoko, and H. Takagi, *Phys. Rev. B* **85**, 214505 (2012).
- [29] J. E. Hoffman, *Rep. Prog. Phys.* **74**, 124513 (2011).
- [30] M. Maltseva and P. Coleman, *Phys. Rev. B* **80**, 144514 (2009).